

# A systematic search for very massive galaxies at $z > 4$

J. S. Dunlop,<sup>★</sup> M. Cirasuolo and R. J. McLure

*SUPA*<sup>†</sup>, *Institute for Astronomy, University of Edinburgh, Royal Observatory, Blackford Hill, Edinburgh EH9 3HJ*

Accepted 2006 December 28. Received 2006 December 21; in original form 2006 June 8

## ABSTRACT

Motivated by the claimed discovery of a very massive galaxy (HUDF-JD2;  $M \simeq 5 \times 10^{11} M_{\odot}$ ) at extreme redshift ( $z = 6.5$ ) within the Hubble Ultra Deep Field (HUDF), we have completed a systematic search for comparably massive galaxies with  $z > 4$  among the 2688 galaxies in our  $K_S < 23.5$  (AB) catalogue within the CDFS/GOODS-South field. This search was conducted using redshift estimates based on the recently completed, uniquely-deep 11-band ( $B, V, i, z, J, H, K_S, 3.6 \mu\text{m}, 4.5 \mu\text{m}, 5.8 \mu\text{m}, 8.0 \mu\text{m}$ ) imaging in this 125-arcmin<sup>2</sup> field,  $\simeq 25$  times larger than the NICMOS HUDF. To ensure completeness, our approach places no special emphasis on the standard  $V$ -drop,  $i$ -drop or  $z$ -drop criteria commonly used to pre-select candidate high-redshift galaxies.

Initial spectral fitting, based on published catalogue SExtractor photometry, led us to conclude that at least 2669 of the galaxies in our sample lie at  $z < 4$ . This list includes several galaxies for which redshifts  $z > 4$  have been previously proposed. We carried out a detailed investigation of the 19 remaining  $z > 4$  candidates, performing aperture photometry on all images, and including marginal detections and formal non-detections in the fitting process. This led to the rejection of a further 13 galaxies to lower redshift. Moreover, subjecting HUDF-JD2 to the same analysis, we find that it almost certainly lies at  $2 < z < 3$ , rather than the extreme redshift favoured by Mobasher et al.

The six remaining candidates appear to be credible examples of galaxies in the redshift range  $z = 4\text{--}6$ , with plausible stellar ages. However, refitting with allowance for extreme values of extinction, we find that, even for these objects, statistically acceptable solutions can be found at  $z < 3$ . In fact, only two galaxies retain formally preferred high-redshift solutions. Moreover, the recently released *Spitzer* MIPS imaging in GOODS-South has revealed that five out of our six final  $z > 4$  candidates are detected at  $24 \mu\text{m}$ . This was also the case for HUDF-JD2, and provides further circumstantial evidence in favour of the moderate-redshift dusty solutions. We conclude that there is no convincing evidence for any galaxy with  $M > 3 \times 10^{11} M_{\odot}$  and  $z > 4$  within the 125-arcmin<sup>2</sup> GOODS-South field. We briefly discuss the implications of this null result, and revised expectations for the much larger (0.8 deg<sup>2</sup>), and deeper near-infrared UKIDSS Ultra Deep Survey now underway with the WFCAM on the UKIRT.

**Key words:** galaxies: evolution – galaxies: formation – cosmology: observations.

## 1 INTRODUCTION

Several hundred convincing galaxy candidates have now been uncovered at  $z \simeq 5\text{--}6.5$  (e.g. Bunker & Stanway 2004; Ouchi et al. 2005; Shioya et al. 2005; Taniguchi et al. 2005; Yan et al. 2005; Bouwens et al. 2006), with a few (arguably less convincing) galaxy candidates even reported at  $z > 7$  (Bouwens et al. 2004). The discovery of such objects has been used to set interesting new constraints

on the cosmic history of star formation density (e.g. Bouwens & Illingworth 2006; Stark et al. 2006), but has not, as yet, presented a serious challenge to current theories of galaxy formation. This is because the masses of essentially all these objects are relatively modest ( $M \simeq 10^{10} M_{\odot}$ ), and the observed large numbers of such objects are consistent with the predictions of at least some current galaxy formation models (e.g. Nagamine et al. 2006).

By contrast, the discovery of even a small number of very massive galaxies at these extreme redshifts can present a stern challenge for both semi-analytic and hydrodynamic galaxy formation models. Indeed, given the steep decline in the predicted number density of high-mass haloes at  $z > 4$  (e.g. Somerville 2005), the discovery

<sup>★</sup>jsd@roe.ac.uk

<sup>†</sup>Scottish Universities Physics Alliance.

of a significant number density of very massive objects at such redshifts has the potential to provide an interesting test of the now well-established paradigm of hierarchical structure growth within  $\Lambda$  cold dark matter ( $\Lambda$ CDM).

For this reason, two recent studies have generated a lot of interest. First, Eyles et al. (2005), in their detailed study of three spectroscopically confirmed Lyman-break galaxies at  $z \simeq 5.5$ –6, reported that these objects already contained a substantial, evolved mass of stars, apparently formed at redshifts as high as  $z \simeq 7.5$ –13.5. Secondly, Mobasher et al. (2005) presented apparently convincing evidence for the existence of an extremely massive galaxy (HUDF-JD2;  $M \simeq 5 \times 10^{11} M_{\odot}$ ) lying within the NICMOS Hubble Ultra Deep Field (HUDF) at the extreme redshift of  $z = 6.5$ . Although this is just one object, its discovery within such a very small area survey, such as the HUDF, is undoubtedly surprising and has already generated considerable interest (e.g. Panagia et al. 2005).

Motivated by the discovery of HUDF-JD2, we decided to revisit our existing redshift determinations for  $K_S$ -band selected galaxies in GOODS-South (Caputi et al. 2004, 2005, 2006), and to conduct a systematic search for the existence of *any* galaxies in this sample at very high redshift ( $z > 4$ ). The key point here is that HUDF-JD2 is sufficiently massive that it is relatively bright in the near-infrared (near-IR), with  $K_S = 23.9$ . Thus, it should be possible to detect comparable objects (less than a factor of 1.5 more massive at  $z \simeq 6.5$ ) within our complete  $K_S < 23.5$  sample of 2898 objects (galaxies and stars) in the GOODS-South field, which covers a solid angle  $\simeq 25$  times larger than that subtended by the NICMOS HUDF. It is also clear that, in this extreme mass domain, the discovery of even one object within the entire GOODS-South field would be extremely important.

Given the apparent evidence for some moderately evolved stellar populations in high-redshift galaxies, and because we wished to search for any galaxies over a relatively wide redshift range  $4 < z < 8$ , we decided not to base our search on strict colour criteria. Such criteria are frequently adopted in the selection of high-redshift galaxies, in order to ensure minimal contamination from low-redshift interlopers (e.g. Bunker & Stanway 2004). However, especially at  $z = 4$ –5, such clean selection inevitably comes at the expense of completeness, and introduces an inevitable bias in favour of the youngest, and hence lowest mass-to-light ratio galaxies. Instead, we updated the data set utilized by Caputi et al. (2006) with the addition of the recently released ISAAC  $H$ -band and complete *Spitzer* four-band IRAC data, and then derived new redshift estimates for all 2688 galaxies in the  $K_S < 23.5$  sample by fitting a range of single- and double-component spectrophotometric models to the full 11-band optical–IR photometry.

The full results of this process are described in Cirasuolo et al. (2006) in which we have utilized this new data set to explore the cosmological evolution of the galaxy mass function out to  $z = 4$ . In this paper, we use this work simply as a starting point for the careful study of the relatively small subsample of galaxies which were found to have even marginally convincing solutions at  $z > 4$ .

This paper is structured as follows. In Section 2, we briefly describe how we have utilized the updated public data set within the GOODS-South field to create a revised, complete sample of 2688 galaxies with  $K_S < 23.5$  and full, aperture-matched 11-band *HST*/ACS+VLT/ISAAC+*Spitzer*/IRAC photometry. In Section 3, we describe the redshift-estimation technique, and demonstrate that it yields robust solutions at the correct redshifts for known, spectroscopically confirmed galaxies at  $z \simeq 5$ –6. In Section 4, we then describe the results of applying this technique to isolate a maximal sample of 32 potential  $z > 4$  galaxies within our GOODS-South

sample, (using 2.8-arcsec-diameter aperture photometry) which was then refined down to a subsample of 19 serious candidates using smaller-aperture SExtractor (Bertin & Arnout 1996) measurements. Section 5 then presents the results of a detailed investigation of the multifrequency data for these remaining 19 candidates, with manual aperture photometry leading to the rejection of a further 13 objects to lower redshift. In this section, we also show that, by subjecting HUDF-JD2 to the same treatment, we find that it does not lie at  $z = 6.5$  (as concluded by Mobasher et al. 2005), but is in fact a dusty, evolved galaxy at  $z \simeq 2.15$ . The final interrogation of our remaining six candidate  $z > 4$  massive galaxies is presented in Section 6. In particular, we explore the robustness of the derived redshifts when the assumed optical extinction is allowed to float up to values as large as  $A_V = 6$ . Finally, in Section 7 we briefly discuss the implications of our results in the context of theoretical models of structure formation.

All optical and IR magnitudes are given in the AB system (Oke & Gunn 1983). Masses and ages have been calculated assuming a cosmological model with  $\Omega_M = 0.3$ ,  $\Omega_{\Lambda} = 0.7$ , and  $H_0 = 70 \text{ km s}^{-1} \text{ Mpc}^{-1}$ .

## 2 DATA AND SAMPLE DEFINITION

### 2.1 New public data

The survey area available for this study is determined by the coverage of the VLT ISAAC  $H$ -band imaging of the GOODS-South field released in 2005 September. These data cover 125 arcmin<sup>2</sup>, for which there already exists complete ISAAC imaging in  $J$ , and  $K_S$ , along with complete *HST* ACS imaging in  $B_{435}$  (three orbits),  $V_{606}$  (2.5 orbits),  $i_{775}$  (2.5 orbits) and  $z_{850}$  (5.0 orbits).

*Spitzer* IRAC imaging, in all four IRAC bands has now also become available for the whole of this field, with the 3.6- and 4.5- $\mu\text{m}$  imaging considered by Caputi et al. (2006) now supplemented by the 5.8- and 8.0- $\mu\text{m}$  imaging.

### 2.2 Final sample properties

The parent sample consists of the 2898 objects in this field which have  $K_S \leq 23.5$  within a 2.8-arcsec-diameter aperture. At this magnitude limit the sample should be essentially 100 per cent complete. Star–galaxy separation (SExtractor stellarity parameter  $> 0.8$  in the ACS  $z$ -band images) led to the rejection of 210 objects as stars, leaving a final complete sample of 2688 galaxies.

Following several recent deep multiobject spectroscopy campaigns (Doherty et al. 2005; Vanzella et al. 2005; Roche et al. 2006; Vanzella et al. 2006), 850 galaxies in our sample now possess reliable spectroscopic redshifts. A further 188 galaxies, with  $R < 22.6$ , can be allocated solid redshifts from the COMBO-17 survey (Wolf et al. 2004). Thus, for 1650 galaxies we required to derive an estimated redshift based on the available, deep, 11-waveband photometry.

### 2.3 Initial multiwavelength photometry

The measurement of a robust 11-waveband spectral energy distribution (SED) for each source in the catalogue is non-trivial because the data span such a wide range in resolution (from  $\simeq 0.1$  arcsec in the *HST*  $B$ -band images, through to  $\simeq 2$  arcsec in the *Spitzer* IRAC 8- $\mu\text{m}$  imaging). To maximize sensitivity at short wavelengths, it is tempting to consider the use of small ( $< 1$  arcsec) apertures for source photometry in the ACS images. However, while most of the flux from genuine high-redshift ( $z > 4$ ) galaxies is likely to lie within

a 1-arcsec aperture, there are obvious dangers in combining small-aperture *HST* photometry with the larger apertures required to obtain a robust estimate of total flux in the near-IR ground-based imaging, and the *Spitzer* IRAC imaging. In particular, unless sufficient care is taken with the aperture corrections, the strength of any putative break between the *J* and  $z_{850}$  filters can be exaggerated, leading to an erroneous conclusion in favour of a very high-redshift galaxy.

To minimize the effect of any such bias, we based our initial photometric catalogue on the use of 2.8-arcsec-diameter apertures for all the optical and near-IR data. For the four *Spitzer* IRAC bands, we also used a 2.8-arcsec-diameter aperture but then applied an aperture correction to estimate the anticipated total flux for a point source (ranging from 0.55 mag at 3.6  $\mu\text{m}$  to 1.0 mag at 8  $\mu\text{m}$ ). As we explain below, once we had used these data to isolate the subset of potential  $z > 4$  galaxies, we considered alternative strategies to push the imaging closer to its photometric limit.

### 3 REDSHIFT ESTIMATION

#### 3.1 Technique

The photometric redshift for each galaxy was computed by fitting the 11 photometric data points (from the *B* band to 8  $\mu\text{m}$ ) with synthetic galaxy templates. These templates were produced using the stellar population synthesis models of Bruzual & Charlot (2003), assuming a Salpeter initial mass function (IMF) with a lower and upper mass cut-off at 0.1 and 100  $M_{\odot}$ , respectively. [We also explored the use of the Jimenez et al. (2004) models, and the Chabrier (2003) IMF, but these yielded inferior fits to the data.]

A range of templates were constructed based on different assumed star formation histories. Specifically, we considered (i) a single instantaneous starburst with passive evolution thereafter, (ii) exponentially declining star formation rates with e-folding times in the range  $0.3 \leq \tau$  (Gyr)  $\leq 15$ , and (iii) two-component burst models (to cope with the possibility of more stochastic star formation histories). In all cases we adopted solar metallicity.

To account for the effects of dust reddening, we adopted the obscuration law of Calzetti et al. (2000). Initially, we allowed *V*-band extinction to range up to  $A_V = 2$ , but ultimately we explored the expanded range  $0 \leq A_V \leq 10$  (see Section 6). We also added a prescription for the Lyman series absorption due to the H I clouds in the inter galactic medium, following Madau (1995).

Some additional information was also utilized to exclude unreasonable redshift solutions. First, the photometric redshift was constrained to lie at  $z \leq 2$  if the source had been detected in the (relatively shallow) *U*-band imaging of the CDFS undertaken as part of the ESO Wide Field Survey (Arnouts et al. 2001). Secondly, a high-redshift solution was excluded if it resulted in a galaxy lying more than 1.3 mag brightwards of the *K* –  $z$  relation defined by the most-luminous radio galaxies (Willott et al. 2003), in effect equivalent to a galaxy more massive than a present-day  $10L^*$  elliptical.

#### 3.2 Tests

Our redshift estimation code has been tested for the  $\simeq 1000$  galaxies in our GOODS-South  $K_S$ -selected sample which possess a reliable spectroscopic or COMBO-17 redshift. As detailed in Cirasuolo et al. (2006), the  $1\sigma$  uncertainty in estimated redshift inferred from this test is  $\delta z / (1 + z) \simeq 0.07$ .

However, of more specific interest for this study is the ability of our method to accurately estimate the redshifts of known objects at  $z > 4$ . To check this, we applied our code to estimate the redshifts

of the four spectroscopically confirmed  $z \simeq 5$ –6 galaxies in the UDF/GOODS field. This is a useful test because the published multiwavelength photometry for these four sources (Eyles et al. 2005; Stark et al. 2006) provides comparable wavelength coverage to the photometry available for our complete GOODS-South sample.

The results of this test are summarized in Table 1, and illustrated in Fig. 1 which shows, for each galaxy, a plot of  $\chi^2$  versus  $z$  (marginalized over age, normalization, and  $A_V$ ) and a comparison of the best-fitting model SED with the broad-band photometry.

Clearly, the code does an excellent job of recovering the redshifts of these galaxies. However, this is arguably a rather easy test, since these are, by nature of their selection, rather clear-cut examples of young Lyman-break galaxies. As discussed further below, and as illustrated by the example of HUDF-JD2 (Mobasher et al. 2005), the situation is inevitably more confused if one is dealing with a potentially more evolved stellar population, with a less blue SED longwards of the Lyman break. Nevertheless, the results shown in Fig. 1 do at least confirm that our multiwavelength SED fitting technique can efficiently and unambiguously identify high-redshift galaxies without recourse to any pre-selection of candidates based on, for example, specific colour criteria.

For completeness, we also note that the masses and ages we have derived for these galaxies are in excellent agreement with those derived by Eyles et al. (2005) and Stark et al. (2006).

### 4 REFINEMENT OF A HIGH-REDSHIFT SAMPLE

#### 4.1 Initial $z > 4$ sample

Initial application of our redshift estimation code to the full 2688-galaxy 11-waveband photometric data set described above yielded formally acceptable solutions at  $z > 4$  for 32 galaxies. In practice, at this stage we aimed to retain all potential  $z > 4$  galaxies for further detailed analysis, and retained any galaxy which displayed even a marginally acceptable solution at  $z > 3.8$ . This, coupled with the initial use of limited reddening and large optical apertures (yielding many formal non-detections in the *HST* data) resulted in an inclusive subset of objects, undoubtedly biased towards high-redshift solutions.

The resulting 32-galaxy subset did not contain any of the objects for which redshifts have been obtained with the VLT (Vanzella et al. 2005, 2006), nor did it include any of the 18 claimed *V*-drop or *I*-drop galaxies within our sample listed by Bremer et al. (2004) and Dickinson et al. (2004), all of which were found to lie at  $z < 3$ . It also contains only one out of the seven galaxies within our sample which are listed as having  $z > 4$  in the GOODS-MUSIC catalogue (Grazian et al. 2006).

The initial derived redshift distribution for these 32 objects is shown in the top panel of Fig. 2.

#### 4.2 Revised $z > 4$ sample after 1-arcsec catalogue search

We next explored the 1-arcsec-diameter aperture *HST* SExtractor catalogue for these 32 sources. This was done to check if any non-detections in the larger aperture became detections with reduced noise. The result of this was the relegation of a further 13 galaxies to lower redshifts, leaving a reduced subset of 19 potential  $z > 4$  galaxies warranting further investigation. The result of this stage in the filtering is shown by the central panel in Fig. 2, and details of the remaining 19 sources are given in Table 2.

**Table 1.** A test of our redshift estimation code at high redshift. Best-fitting model parameters are given for our spectral fits to the broad-band photometry of the four spectroscopically confirmed  $z = 5\text{--}6$  galaxies in the HUDF/GOODS-South field (Bunker et al. 2003; Stanway et al. 2004) for which seven-band photometry has been published by Eyles et al. (2005) and Stark et al. (2006). For each object, we give the best-fitting parameter values both for the best-fitting model with an exponentially declining star formation rate and for the best-fitting simple burst model. The fits are plotted in Fig. 1, along with  $\chi^2$  versus estimated redshift, marginalized over age, normalization, varied star formation history, and extinction.

Source	$z_{\text{spec}}$	$z_{\text{est}}$	Model type	$\chi^2$	Age (Gyr $^{-1}$ )	$A_V$	Mass ( $10^{10} M_{\odot}$ )
SBM03#1	5.83	$5.70 \pm 0.07$	$\tau = 0.3$ Gyr	5.26	0.64	0.0	3.2
		$5.40 \pm 0.15$	Burst	11.63	0.10	0.0	1.4
SBM03#3	5.78	$5.70 \pm 0.07$	$\tau = 1.0$ Gyr	9.01	0.91	0.0	6.5
		$5.55 \pm 0.15$	Burst	19.26	0.06	0.0	1.6
GLARE#3001	5.79	$5.75 \pm 0.12$	$\tau = 0.3$ Gyr	3.80	0.06	0.6	1.1
		$5.62 \pm 0.15$	Burst	4.52	0.06	0.0	0.3
32_8020	5.55	$5.26 \pm 0.10$	$\tau = 0.3$ Gyr	9.64	0.91	0.0	15.8
		$4.76 \pm 0.15$	Burst	36.23	0.06	0.6	5.6

## 5 DETAILED STUDY OF THE FINAL HIGH-REDSHIFT SAMPLE

### 5.1 Direct aperture photometry

At this point in the analysis, the values adopted for limiting magnitudes in the case of SExtractor non-detections become crucial. In

particular, the extent to which a high-redshift solution is favoured can be critically dependent on how any apparent non-detections are treated.

One way to tackle this is the approach taken by Mobasher et al. (2005) in their analysis of HUDF-JD2. Faced with apparent non-detection of this object in the deep HUDF ACS optical imaging, they adopted  $2\sigma$  upper limits of  $B = 30.6$ ,  $V = 31.0$ ,  $i_{775} = 30.9$ ,  $z_{850} =$

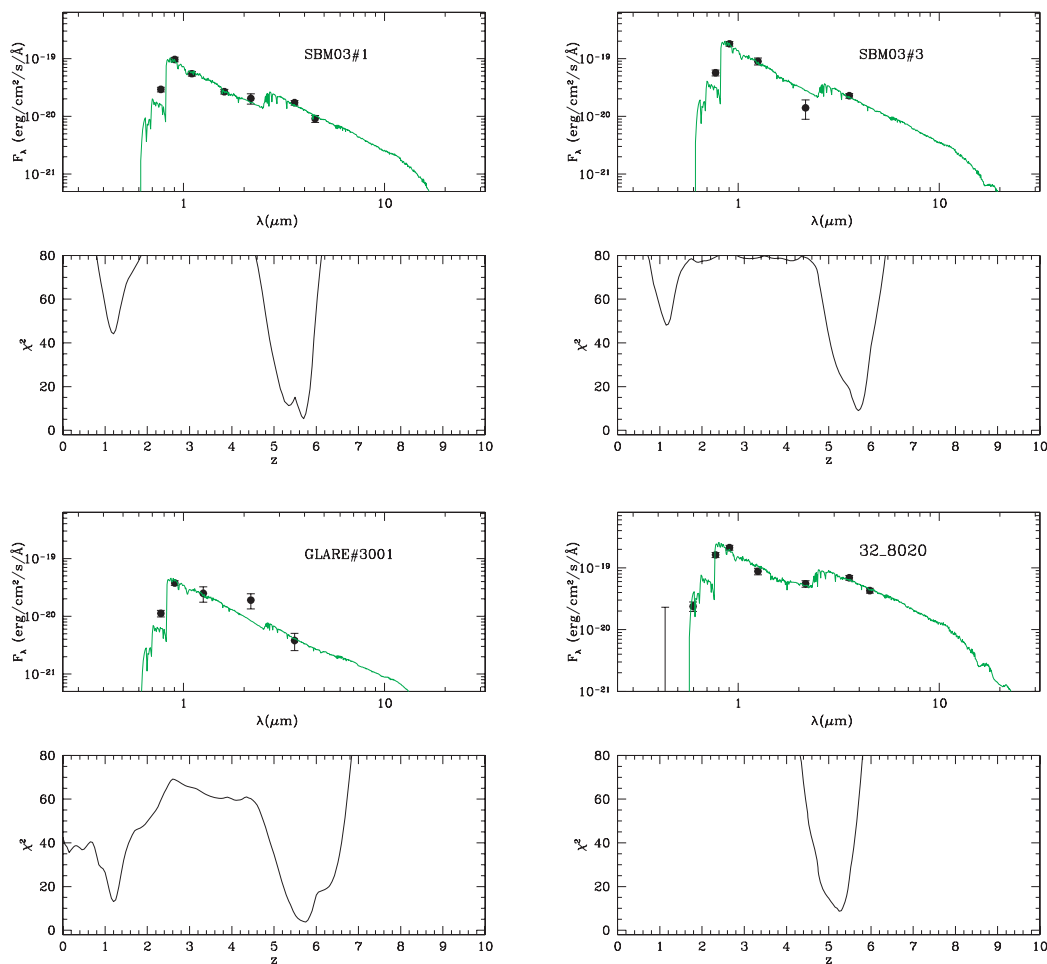


**Figure 1.** Spectral fits and  $\chi^2$  versus redshift  $z$  for the four galaxies in the HUDF and GOODS-South field with measured spectroscopic redshifts  $z > 5$  (Bunker et al. 2003; Stanway et al. 2004), and published seven-band photometry as tabulated by Eyles et al. (2005) and Stark et al. (2006). Details of the model fits, and a comparison of estimated and spectroscopic redshifts are given in Table 1.

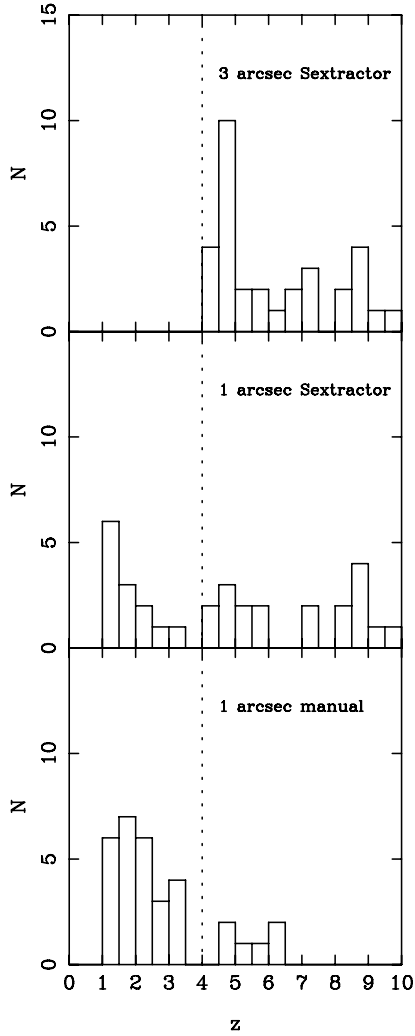


**Figure 2.** Progressive refinement of the estimated redshift distribution of the initial 32-source  $z > 4$  candidate list as the photometric measurements are pushed closer to the limit allowed by the imaging data. The top panel shows the redshift distribution based on initial 2.8-arcsec-diameter aperture magnitudes, and adopting formal limits for the non-detections in the ACS optical bands. The middle panel shows the impact of moving to smaller (1-arcsec-diameter) SExtractor magnitudes. The bottom panel shows the effect of refitting the 19 objects which lie at  $z > 4$  in the middle panel to the manual aperture photometry tabulated in Tables 3 and 4. The six objects which apparently remain at  $z > 4$  are discussed in detail in Sections 5.3 and 6.

30.3, within their chosen 0.9-arcsec diameter aperture. We note here that at least some of these limits seem rather deep compared to the limits adopted by some other authors working with HUDF data. For example, Bouwens et al. (2004), in their search for  $z_{850}$ -drop

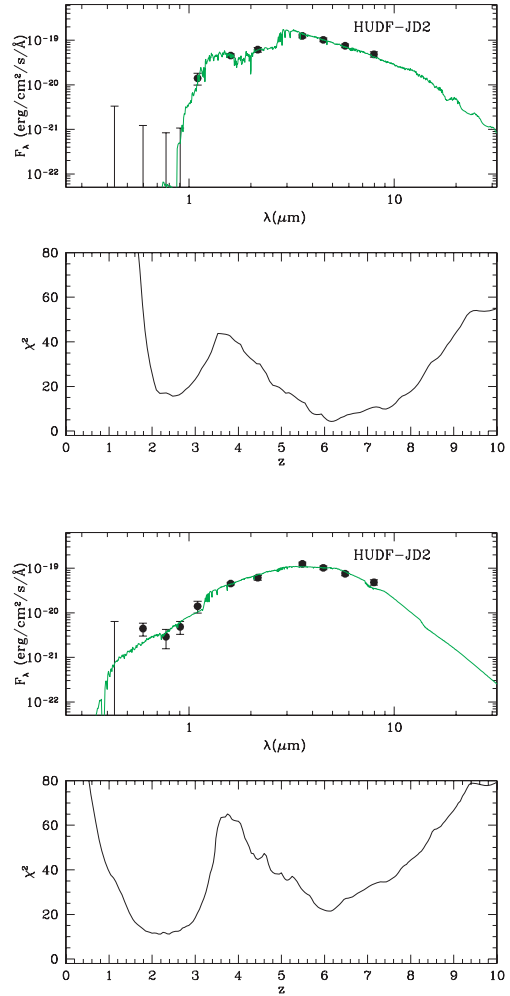


**Figure 3.** Spectral fits and  $\chi^2$  versus redshift  $z$  for HUDF-JD2. The top panel shows the result of applying our model fitting to the photometric data published by Mobasher et al. (2005). The lower panel shows the result of fitting to our own independent photometry, as discussed in Section 5.2. Best-fitting model parameters for both sets of data are given in Table 2.

galaxies in the HUDF, appear to have found a typical  $2\sigma$  limit of  $z_{850} > 29.8$  within a 0.6-arcsec-diameter aperture, which converts to  $z_{850} > 29.4$  for a 0.9-arcsec-diameter aperture, almost a magnitude shallower than that adopted by Mobasher et al. (2005).

We investigated the effect of calculating equivalent limits for our GOODS non-detections (i.e. scaling the Mobasher et al. values to a 1-arcsec-diameter aperture, and correcting for the GOODS-to-HUDF orbit ratio in each band). This leads to the conclusion that our adopted  $2\sigma$  limits should be  $B = 28.9$ ,  $V = 29.2$ ,  $i_{775} = 28.6$ ,  $z_{850} = 28.3$ .

**Table 2.** Estimated redshifts and other model parameter values for fits to the observed SED of HUDF-JD2 using (i) the published 11-waveband photometry (Mobasher et al. 2005) and (ii) the revised photometry described in Section 5.2.

Source	$z_{\text{est}}$	Model type	$\chi^2$	Age (Gyr $^{-1}$ )	$A_V$	Mass ( $10^{11} M_{\odot}$ )
HUDF-JD2: published photometry	$6.20 \pm 0.20$	Burst	4.4	0.57	0.0	6.0
HUDF-JD2: revised photometry	$2.15 \pm 0.30$	Burst	10.9	0.10	3.8	0.8

However, as illustrated in the central panel of Fig. 2, the adoption of such limits would lead us to the conclusion that many of our remaining 19 sources lie at very high redshifts. Faced with such a radical conclusion, we decided to abandon the inferred detection limits, and perform manual aperture photometry for all 19 galaxies to establish the true level of signal and noise, so that even the apparent SExtractor non-detections could be properly incorporated within the  $\chi^2$  fitting in a consistent manner.

For consistency, we therefore decided to also subject HUDF-JD2 to the same type of analysis.

## 5.2 HUDF2 revisited

In the top panel of Fig. 3, we show our own, independent fit to the photometry for HUDF-JD2 published by Mobasher et al. (2005). Our preferred redshift of  $z = 6.2 \pm 0.2$  is consistent with the value of  $z = 6.5$  derived by Mobasher et al. (2005), and we agree that the high-redshift solution is significantly favoured over the alternative option of a dust-obscured galaxy at  $z \simeq 2-3$ . The parameter values for our best-fitting solution to the published photometry are given in Table 2.

However, performing our own manual photometry on the public HUDF images, through a 0.9-arcsec-diameter aperture (as adopted by Mobasher et al.), we derive  $B > 29.9$  ( $1\sigma$ ),  $V = 29.6 \pm 0.35$ ,  $i_{775} = 29.5 \pm 0.5$  and  $z_{850} = 28.6 \pm 0.35$ . None of these highly marginal detections could, in isolation, be described as very convincing. However, their cumulative effect on the best-fitting solution is dramatic, as illustrated in the lower panel of Fig. 3. The best-fitting result is now at  $z = 2.15$ , and the high-redshift solution is formally excluded. The parameter values for our best-fitting solution to this revised photometry are also given in Table 2. We conclude, therefore, that HUDF-JD2 very likely lies at  $z < 3$ , and not at  $z > 6$ .

## 5.3 Final photometry and redshift distribution

The positions, and final 11-waveband photometry for the 19 remaining  $z > 4$  candidates are given in Tables 3 and 4. Optical magni-

tudes are based on manual photometry through a 1-arcsec-diameter aperture as described above, with errors given in magnitudes if the signal-to-noise ratio is greater than 3, and as a fractional error in flux if the ‘detection’ is less significant. To avoid bias, the  $J$ ,  $H$ ,  $K_S$  values have been re-derived also using a 1-arcsec-diameter aperture, with a minimal (effectively stellar) aperture correction of  $-0.5$  mag applied to correct for missing flux. In practice, there is inevitably a small systematic error connected with such aperture corrections, and so for the purpose of spectral fitting we adopted a minimum error of 0.1 mag for the  $J$ ,  $H$ ,  $K_S$  photometry listed in Table 4.

The estimated redshifts resulting from fitting to the final photometry for these 19 galaxies are listed in Table 5, with the resulting redshift distribution shown in the bottom panel of Fig. 2. Clearly all 19 of these galaxies are interesting objects, with a sharp decline in flux-density shortwards of the  $J$  band, but now only six galaxies retain credible solutions at  $z > 4$ . Plots of  $\chi^2$  versus redshift (marginalized over age, extinction and star formation history) and the best-fitting model SEDs for these six galaxies are shown in Fig. 4.

For comparison, we have also listed in Table 5 the estimated redshifts for these 19 galaxies recently released by Grazian et al. (2006) as part of the GOODS-MUSIC project. We have also applied our own spectral fitting technique to the GOODS-MUSIC photometry for these objects, to allow us to explore the extent to which any disagreements may depend on photometry or model fitting. An inspection of Table 5 shows that, for many of these galaxies, the agreement between all three redshift estimates is excellent. However, there are also obvious differences. Specifically, only one of these objects has a redshift  $z > 4$  in the GOODS-MUSIC list, and our own solution for this object with either photometry set lies at  $z < 4$ . Before discussing further the likely explanation for this apparent disagreement at high redshift, we describe below the result of our final analysis of our own remaining subset of six potential  $z > 4$  candidates.

## 6 MASSIVE GALAXIES AT HIGH REDSHIFT?

The model fits, and plots of  $\chi^2$  versus redshift shown in Fig. 4 were derived with dust extinction limited to  $A_V < 2$ . As detailed in Table 6,

**Table 3.** Positions and 1-arcsec-diameter aperture *HST* ACS optical magnitudes for the 19 candidate  $z > 4$  galaxies in our GOODS-South sample. Errors are given in magnitudes if the signal-to-noise ratio is greater than 3, and as a percentage error in flux density if the ‘detection’ is less significant.  $1\sigma$  limits are given when the detected flux density was zero or negative (see Section 5.3).

Name	RA (J2000) ( <sup>h</sup> <sup>m</sup> <sup>s</sup> )	Dec. (J2000) ( <sup>o</sup> <sup>'</sup> <sup>"</sup> )	$B$	$V$	$i_{775}$	$z_{850}$
1865	03 32 12.87	-27 46 40.9	29.3 (180 percent)	29.7 (130 percent)	27.6 (70 percent)	26.8 $\pm$ 0.30
2028	03 32 22.53	-27 49 32.6	29.0 (150 percent)	27.0 $\pm$ 0.20	26.3 $\pm$ 0.20	26.3 $\pm$ 0.10
2336	03 32 25.25	-27 52 30.3	> 29.1	28.8 (80 percent)	27.9 (55 percent)	28.1 (80 percent)
2351	03 32 54.75	-27 51 13.8	> 28.7	29.0 (160 percent)	28.4 (160 percent)	27.5 (100 percent)
2476	03 32 37.86	-27 52 01.3	> 28.8	> 29.0	26.8 $\pm$ 0.25	26.1 $\pm$ 0.20
2507	03 32 19.67	-27 46 02.0	28.9 (120 percent)	> 29.5	> 28.6	27.8 (65 percent)
2600	03 32 38.34	-27 51 01.0	28.0 (70 percent)	27.8 $\pm$ 0.35	27.2 $\pm$ 0.30	27.0 (45 percent)
2609	03 32 56.10	-27 52 05.0	28.3 (60 percent)	28.1 (50 percent)	27.1 $\pm$ 0.18	26.3 $\pm$ 0.20
2694	03 32 21.99	-27 51 11.9	28.3 (70 percent)	28.7 (70 percent)	27.7 (60 percent)	28.9 (200 percent)
2869	03 32 17.99	-27 50 52.7	28.1 (70 percent)	27.25 $\pm$ 0.25	26.1 $\pm$ 0.15	26.1 $\pm$ 0.30
2895	03 32.16.83	-27 49 07.7	29.7 (250 percent)	28.6 (50 percent)	27.6 (60 percent)	27.2 (70 percent)
2957	03 32 37.06	-27 44 19.1	28.8 (180 percent)	28.9 (70 percent)	28.4 (130 percent)	26.9 (55 percent)
2958	03 32 42.08	-27 41 41.3	> 29.1	> 28.8	> 28.3	> 28.6
3021	03 32 27.14	-27 53 11.6	> 28.7	28.2 (75 percent)	26.7 $\pm$ 0.35	26.8 (35 percent)
3037	03 32 28.21	-27 51 16.2	> 29.1	27.3 $\pm$ 0.20	26.6 $\pm$ 0.15	26.4 $\pm$ 0.25
3048	03 32 19.57	-27 41 39.9	> 28.2	> 29.1	27.0 (50 percent)	26.8 $\pm$ 0.33
3087	03 32 54.81	-27 51 38.8	27.8 (40 percent)	27.8 (40 percent)	28.5 (50 percent)	26.8 $\pm$ 0.25
3088	03 32 39.13	-27 51 05.0	28.5 (120 percent)	28.9 (65 percent)	26.8 $\pm$ 0.15	27.9 (60 percent)
3122	03 32 21.69	-27 42 42.3	> 29.1	27.9 (40 percent)	28.7 (150 percent)	27.9 (80 percent)

**Table 4.** IR photometry for the 19 candidate  $z > 4$  galaxies.  $J, H, K_S$  magnitudes have been re-derived from the public VLT ISAAC imaging using 1-arcsec-diameter apertures, and applying a point-source correction of  $-0.5$  mag. The *Spitzer* IRAC magnitudes have also been corrected to account for the point spread function, and typical errors adopted for all objects at each waveband.

Name	$J$	$H$	$K_S$	$3.6 \mu\text{m}$	$4.5 \mu\text{m}$	$5.8 \mu\text{m}$	$8.0 \mu\text{m}$
1865	$24.33 \pm 0.13$	$23.52 \pm 0.06$	$22.62 \pm 0.05$	$20.96 \pm 0.20$	$20.72 \pm 0.20$	$20.64 \pm 0.30$	$21.02 \pm 0.30$
2028	$23.86 \pm 0.07$	$23.15 \pm 0.07$	$22.66 \pm 0.04$	$20.55 \pm 0.20$	$20.77 \pm 0.20$	$20.47 \pm 0.30$	$20.60 \pm 0.30$
2336	$24.98 \pm 0.17$	$23.86 \pm 0.12$	$22.96 \pm 0.04$	$21.29 \pm 0.20$	$20.81 \pm 0.20$	$20.34 \pm 0.30$	$20.30 \pm 0.30$
2351	$25.10 \pm 0.34$	$23.64 \pm 0.13$	$22.98 \pm 0.07$	$21.33 \pm 0.20$	$21.10 \pm 0.20$	$21.04 \pm 0.30$	$21.26 \pm 0.30$
2476	$23.99 \pm 0.08$	$23.30 \pm 0.08$	$22.96 \pm 0.05$	$22.14 \pm 0.20$	$21.92 \pm 0.20$	$21.96 \pm 0.30$	$22.26 \pm 0.30$
2507	$25.48 \pm 0.26$	$24.41 \pm 0.16$	$23.04 \pm 0.04$	$21.20 \pm 0.20$	$20.77 \pm 0.20$	$20.25 \pm 0.30$	$20.43 \pm 0.30$
2600	$25.20 \pm 0.22$	$23.83 \pm 0.09$	$22.93 \pm 0.05$	$21.59 \pm 0.20$	$21.26 \pm 0.20$	$21.23 \pm 0.30$	$21.48 \pm 0.30$
2609	$24.63 \pm 0.14$	$23.42 \pm 0.08$	$23.12 \pm 0.06$	$21.78 \pm 0.20$	$21.47 \pm 0.20$	$21.64 \pm 0.30$	$21.71 \pm 0.30$
2694	$25.87 \pm 0.41$	$24.59 \pm 0.22$	$23.08 \pm 0.05$	$21.31 \pm 0.20$	$20.88 \pm 0.20$	$20.47 \pm 0.30$	$20.78 \pm 0.30$
2869	$24.89 \pm 0.20$	$24.06 \pm 0.15$	$23.18 \pm 0.06$	$21.57 \pm 0.20$	$21.37 \pm 0.20$	$21.33 \pm 0.30$	$20.41 \pm 0.30$
2895	$25.01 \pm 0.18$	$24.13 \pm 0.15$	$22.99 \pm 0.04$	$21.68 \pm 0.20$	$21.57 \pm 0.20$	$21.73 \pm 0.30$	$21.85 \pm 0.30$
2957	$25.80 \pm 0.33$	$24.65 \pm 0.15$	$23.05 \pm 0.04$	$21.89 \pm 0.20$	$21.52 \pm 0.20$	$21.06 \pm 0.30$	$21.32 \pm 0.30$
2958	$25.51 \pm 0.33$	$24.56 \pm 0.23$	$23.34 \pm 0.09$	$21.34 \pm 0.20$	$20.95 \pm 0.20$	$20.48 \pm 0.30$	$20.44 \pm 0.30$
3021	$25.27 \pm 0.19$	$24.29 \pm 0.15$	$23.46 \pm 0.07$	$21.77 \pm 0.20$	$21.49 \pm 0.20$	$21.09 \pm 0.30$	$21.19 \pm 0.30$
3037	$24.60 \pm 0.12$	$24.01 \pm 0.12$	$23.39 \pm 0.07$	$22.38 \pm 0.20$	$22.13 \pm 0.20$	$21.53 \pm 0.30$	$22.18 \pm 0.30$
3048	$25.60 \pm 0.31$	$24.26 \pm 0.23$	$23.49 \pm 0.08$	$21.69 \pm 0.20$	$21.29 \pm 0.20$	$20.77 \pm 0.30$	$20.93 \pm 0.30$
3087	$25.30 \pm 0.29$	$24.16 \pm 0.17$	$23.22 \pm 0.07$	$21.83 \pm 0.20$	$21.55 \pm 0.20$	$21.01 \pm 0.30$	$21.26 \pm 0.30$
3088	$24.60 \pm 0.12$	$24.19 \pm 0.15$	$23.33 \pm 0.08$	$21.92 \pm 0.20$	$21.64 \pm 0.20$	$21.62 \pm 0.30$	$22.03 \pm 0.30$
3122	$27.21 \pm 0.16$	$23.85 \pm 0.14$	$23.28 \pm 0.09$	$21.81 \pm 0.20$	$21.54 \pm 0.20$	$21.20 \pm 0.30$	$21.35 \pm 0.30$

most of these ‘high-redshift’ solutions are statistically acceptable, and yield plausible values for many of the model parameters (e.g. ages less than the age of the universe at the epoch of interest). However, while obviously not as surprising as the claimed discovery of HUDF-JD2, the existence of six galaxies at  $z > 4$  with masses  $M > 3 \times 10^{11} M_{\odot}$  within a  $125\text{-arcmin}^2$  field is still unexpected.

Therefore, as a final step in the analysis we refitted these six galaxies with extinction now allowed to range up to  $A_V \simeq 10$ . The results of this process are illustrated in the contour plots shown in Fig. 5. Acceptable, alternative low-redshift solutions are now found for all six galaxies and, as detailed in Table 6, are now formally preferred for all except two galaxies (2507 and 3048), and even in these two cases the lower-redshift solution is formally acceptable.

**Table 5.** Re-estimated redshifts for the 19 candidate  $z > 4$  galaxies in our GOODS-South sample. Column 2 gives the estimated redshift (and associated uncertainty) which we have derived by applying the technique described in Section 3.1, to the revised photometric data tabulated in Tables 3 and 4. The values of minimum  $\chi^2$  for these fits are given in column 3. In columns 4 and 5, we give the corresponding object IDs and estimated redshifts recently published by Grazian et al. (2006), as part of the GOODS-MUSIC project. In column 6, we give a third estimate of the redshift for each object, this time applying our own technique to the photometric data published by Grazian et al. (2006). Column 7 gives the values of minimum  $\chi^2$  for these fits, many of which are very large (apparently due to problems in fitting some of the claimed  $U$ -band detections in the GOODS-MUSIC catalogue).

Source	$z_{\text{est1}}$ ( $1\sigma$ range)	$\chi^2$	MUSIC ID	MUSIC $z_{\text{est}}$	$z_{\text{est2}}$ ( $1\sigma$ range)	$\chi^2$
1865	5.02 (4.87–5.17)	8.82	30093	2.04	2.00 (1.95–2.10)	72.03
2028	1.95 (1.80–2.10)	42.30	30120	1.97	1.85 (1.80–1.95)	60.69
2336	6.22 (6.07–6.45)	12.73	30199	2.73	3.65 (3.25–3.85)	2.77
2351	1.88 (1.80–2.25)	5.15	30142	1.84	1.85 (1.80–1.95)	25.34
2476	1.65 (1.50–1.80)	6.02	30160	1.59	1.70 (1.50–1.80)	9.53
2507	4.87 (4.72–5.10)	2.20	30049	2.21	1.90 (1.70–2.20)	2.13
2600	2.18 (1.95–2.33)	1.39	30106	2.05	2.15 (2.05–2.25)	78.35
2609	2.33 (2.18–2.40)	10.79	30146	2.06	2.15 (2.05–2.25)	27.48
2694	2.93 (2.55–3.08)	5.88	30114	2.57	3.45 (3.00–3.90)	6.60
2869	3.30 (3.08–3.45)	10.08	30115	1.88	1.55 (1.45–1.65)	65.62
2895	1.73 (1.58–1.88)	4.42	30123	1.94	2.00 (1.75–2.45)	4.24
2957	3.45 (3.30–3.83)	3.81	30048	4.66	3.75 (3.50–4.30)	1.49
2958	6.07 (4.95–6.30)	1.49	30009	1.73	1.95 (1.35–2.35)	0.71
3021	3.00 (2.78–3.23)	8.33	30175	2.44	2.20 (2.10–2.30)	21.98
3037	2.25 (2.10–2.40)	9.39	5177	2.73	1.75 (1.65–1.89)	45.31
3048	4.87 (4.72–5.10)	5.83	30036	2.62	2.45 (2.10–2.70)	3.64
3087	2.18 (1.88–2.33)	12.44	30145	2.53	1.95 (1.75–2.10)	17.55
3088	6.00 (5.85–6.37)	14.14	30097	1.91	1.45 (1.40–1.55)	14.48
3122	2.63 (2.25–2.85)	8.98	30032	3.54	2.65 (2.45–2.85)	25.74

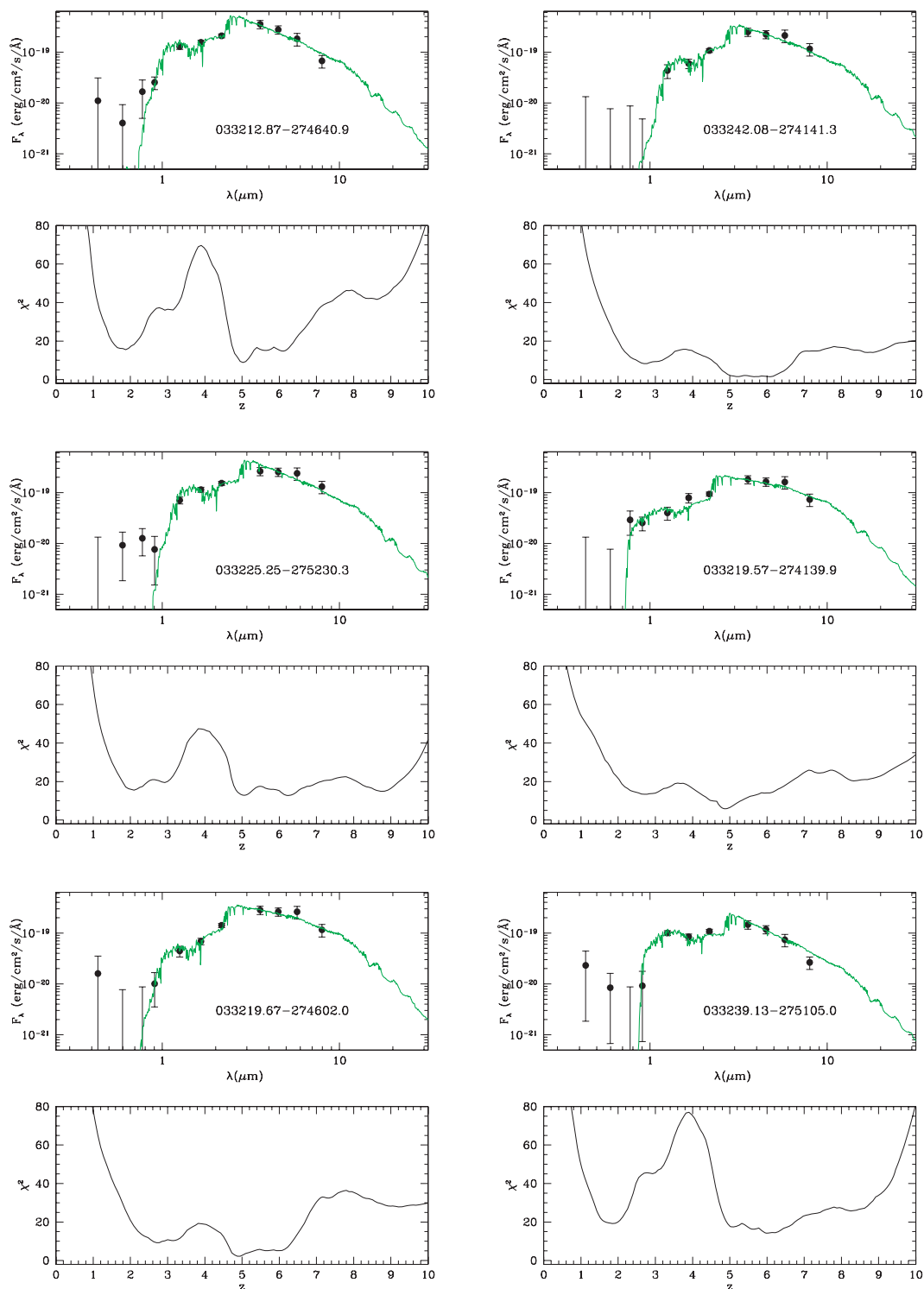


**Figure 4.** Spectral fits and  $\chi^2$  versus estimated redshift  $z$  for the six galaxies in our GOODS-South sample which still have plausible solutions at  $z > 4$  after the sample refinement process described in Section 5. Best-fitting model parameter values are given in Table 6. For  $A_V < 2$ , the high-redshift solutions shown here are formally preferred.

It clearly remains possible that one or more of these six galaxies lies at extreme redshift, but a number of factors mitigate against this conclusion. First, given equally acceptable solutions at  $z \simeq 2$  (with moderate mass but high  $A_V$ ) and  $z \simeq 5$  (with high mass and low  $A_V$ ) the balance of other probabilities clearly favours the low-

redshift option. Secondly, during the completion of this work, the *Spitzer* MIPS 24- $\mu\text{m}$  catalogue for the GOODS-South field was released to the public (Dickinson et al., in preparation). This catalogue contains 24- $\mu\text{m}$  detections for five out of the six galaxies listed in Table 6 (all except 3088). Clearly, such a high detection rate at

**Table 6.** Best-fitting model parameter values for the final six candidate high-redshift objects. The values for the physical parameters, and the value of minimum  $\chi^2$  is given for both the putative high-redshift (low  $A_V$ ) and the moderate-redshift (high  $A_V$ ) solution in each case. The locations of these solutions on the  $A_V$ - $z$  plane are illustrated in Fig. 5.

Source	RA (J2000) ( <sup>h</sup> <sup>m</sup> <sup>s</sup> )	Dec. (J2000) ( <sup>o</sup> <sup>'</sup> <sup>"</sup> )	$z_{\text{est}}$ ( $1\sigma$ range)	Model type	$\chi^2$	Age (Gyr <sup>-1</sup> )	$A_V$	Mass ( $10^{11} M_{\odot}$ )
1865	03 32 12.87	−27 46 40.9	5.02 (4.87–5.17)	Burst	8.82	0.56	0.0	6.0
				Burst	5.20	0.13	3.6	0.9
2336	03 32 25.25	−27 52 30.3	6.22 (6.07–6.45)	Burst	12.73	0.56	0.0	16.6
				Burst	4.80	0.13	3.6	2.0
2507	03 32 19.67	−27 46 02.0	4.87 (4.72–5.10)	Burst	2.20	0.57	0.8	11.2
				$\tau = 15$ Gyr	2.43	0.20	4.8	0.8
2958	03 32 42.08	−27 41 41.3	6.07 (4.95–6.30)	Burst	1.49	0.63	0.2	15.8
				Burst	3.03	0.18	4.6	1.9
3048	03 32 19.57	−27 41 39.9	4.87 (4.72–5.10)	Burst	5.83	0.31	1.2	5.9
				$\tau = 0.3$ Gyr	2.39	0.07	3.6	0.4
3088	03 32 39.13	−27 51 05.0	6.00 (5.85–6.37)	Burst	14.14	0.40	0.0	2.8
				Burst	12.46	0.20	2.8	0.6

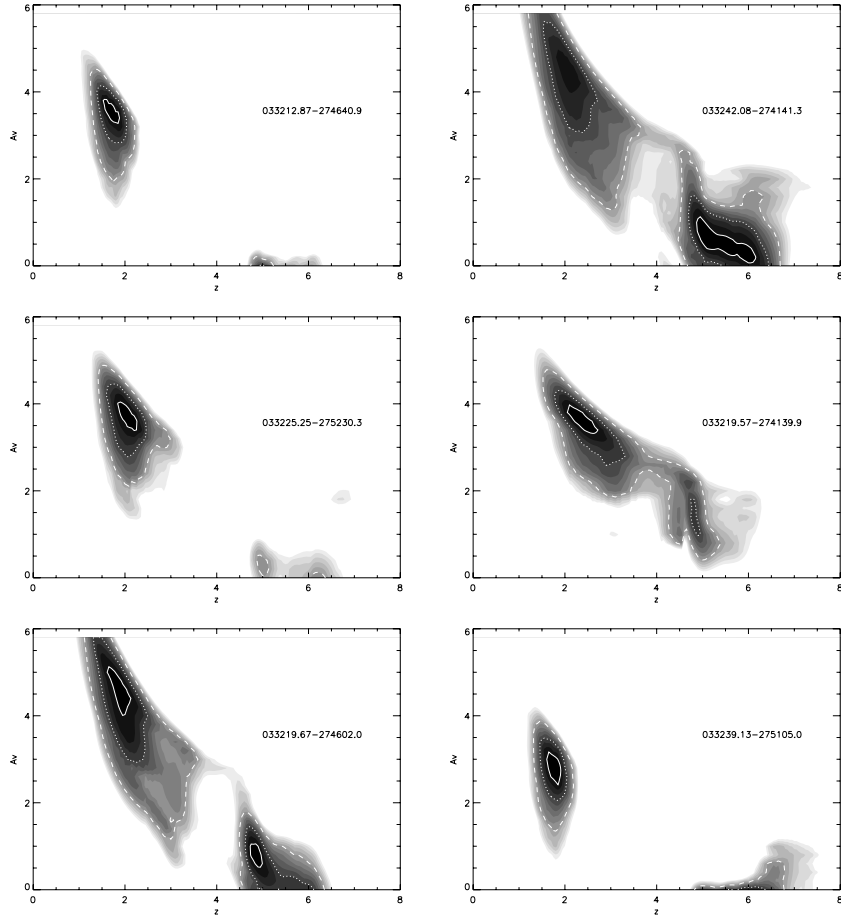


**Figure 5.** Likelihood contours illustrating the location of acceptable fits on the  $A_V$ - $z$  plane for the six objects in our GOODS-South sample with putative redshifts  $z > 4$ . Allowing for large values of extinction, it can be seen that, for all six objects, alternative solutions exist at  $z \simeq 2$ . Contours are shown at intervals of  $\Delta\chi^2 = 1, 4,$  and  $9$  above the minimum value of  $\chi^2$ . The best-fitting values of the model parameters for both the high-redshift and the low-redshift solutions are given in Table 6.

mid-IR wavelengths strongly supports the lower redshift dusty solutions for these objects (we note that HUDF-JD2 was also detected at  $24 \mu\text{m}$ ; Mobasher et al. 2005). Thirdly, our own re-analysis of HUDF-JD2, and the discrepancy between the GOODS-MUSIC redshift estimates and our own results for several of these putative

high-redshift galaxies, serves to demonstrate just how sensitive any conclusion in favour of  $z > 4$  can be to the treatment of marginal and non-detections in the optical wavebands. As demonstrated by Fig. 1, this is a much less serious issue for young/blue high-redshift candidates for which an acceptable lower-redshift dust-obscured

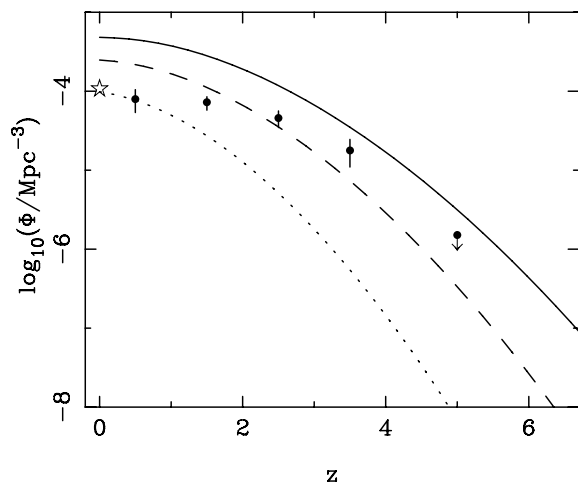


**Figure 6.** A comparison of our best estimate of the evolution of the comoving number density of galaxies with stellar mass  $M > 3 \times 10^{11} M_{\odot}$  with the predicted evolution of the comoving number density of virialized dark matter haloes above three different mass thresholds (as derived from modified Press–Schechter theory; Percival, private communication). The data points for the redshift bins  $0 < z < 1$ ,  $1 < z < 2$ ,  $2 < z < 3$  and  $3 < z < 4$  are derived from the analysis of Cirasuolo et al. (2006) (updated from Caputi et al. 2006), while the reference point at  $z = 0$  has been derived by the appropriate integration of the galaxy mass function provided by Cole et al. (2001) (assuming a Salpeter IMF). The result of the unsuccessful search at  $z > 4$  described here is illustrated by the upper limit plotted at  $z = 5$ , which represents the comoving number density in the redshift bin  $4 < z < 6$  if one out of the six final high-redshift candidates listed in Table 6 really does lie within this high-redshift bin. The curves show the comoving number density of virialized dark matter haloes with  $M > 5 \times 10^{12} M_{\odot}$  (solid line),  $M > 1 \times 10^{13} M_{\odot}$  (dashed line) and  $M > 2.5 \times 10^{13} M_{\odot}$  (dotted line). The last (most massive) of these curves was deliberately chosen to coincide with the data point at  $z = 0$ , and implies a dark matter-to-stellar mass ratio of  $\simeq 80$  for these most-massive galaxies in the present-day universe.

solution often does not exist. However, the results presented here for redder objects serve to illustrate just how hard it will be to unambiguously identify older (and hence potentially more massive) objects at extreme redshifts on the basis of spectral fitting to even the most-comprehensive photometric data set.

## 7 DISCUSSION

To illustrate the implications of this failed search for high-mass galaxies at  $z > 4$ , we show, in Fig. 6, a plot of the comoving number density of galaxies with mass  $M > 3 \times 10^{11} M_{\odot}$  within the GOODS-South field, as a function of redshift. This limit simply corresponds to the lowest mass found for the high-redshift solutions to the six galaxies listed in Table 6.

The data points for the redshift bins  $0 < z < 1$ ,  $1 < z < 2$ ,  $2 < z < 3$ , and  $3 < z < 4$  are derived from the analysis of Cirasuolo et al. (2006) (updated from Caputi et al. 2006), while the reference point at  $z = 0$  has been derived by the appropriate integration of the galaxy mass function provided by Cole et al. (2001) (assuming a Salpeter IMF). The result of the unsuccessful search at  $z > 4$  described here is illustrated by the upper limit plotted at  $z = 5$ , which represents the comoving number density in the redshift bin  $4 < z < 6$  if one out of the six final high-redshift candidates listed in Table 6 really does lie within this high-redshift bin. Also plotted in this figure is the comoving number density of virialized dark matter haloes above

three different mass thresholds, as derived from modified Press–Schechter theory (Percival, private communication).

Several features of this diagram are worthy of comment. First, at no redshift does the number density of high-mass galaxies present a fundamental problem for  $\Lambda$ CDM; the number density of potential dark matter haloes (10–20 times more massive than the stellar masses of the galaxies) clearly exceeds the inferred number density of the massive galaxies.

Nevertheless, out to redshift  $z \simeq 3$ , the number density of these most-massive galaxies changes only slowly (compared to the dark matter curves) and hence, for this class of galaxies, the inferred dark matter-to-stellar mass ratio appears to evolve from  $\simeq 80$  at  $z \simeq 0$  to  $\simeq 20$  at  $z \simeq 3.5$ . Such inferred values do not appear unreasonable (see, for example, Mandelbaum et al. 2006), and this apparent evolution of the dark matter-to-stellar mass ratio can be viewed as yet another manifestation of ‘downsizing’ or apparently ‘anti-hierarchical’ galaxy formation (e.g. Heavens et al. 2004).

However, the upper limit derived here indicates that this ‘anti-hierarchical’ behaviour does not persist beyond  $z \simeq 4$ , and that, at higher redshift, the number density of massive galaxies drops off more rapidly (or possibly more rapidly) than the number density of potential host dark matter haloes.

An improved measurement of the comoving number density of these rare high-mass galaxies at high-redshift clearly requires a substantially larger survey than the  $125 \text{ arcmin}^2$  covered by the GOODS-South multiwavelength imaging. The first such survey of the necessary depth and area is now underway. This is the UKIDSS Ultra Deep Survey (UDS), which covers  $0.8 \text{ deg}^2$ , and is designed to ultimately reach a  $K$ -band  $5\sigma$  detection limit of  $K = 25$  (AB). This survey will therefore cover 25 times the area of GOODS-South, to a magnitude limit substantially deeper than the  $K_S$ -limit of the GOODS-South survey analysed here. A failure to find any galaxies with  $M > 3 \times 10^{11} M_{\odot}$  and  $z > 4$  within the UKIDSS UDS would move the upper limit shown at  $z \simeq 5$  in Fig. 6 down by over an order of magnitude. A first analysis, based on the UKIDSS early data release, has provided evidence for a number of moderately massive galaxies at  $z > 5$ , but as yet has not revealed any as massive as  $M > 3 \times 10^{11} M_{\odot}$  (McLure et al. 2006).

## ACKNOWLEDGMENTS

This work was based in part on observations with the NASA/ESA *Hubble Space Telescope*, obtained at the Space Telescope Science Institute, which is operated by the Association of Universities for Research in Astronomy, Inc. under NASA contract No. NAS5-26555. MC acknowledges the support of the PPARC, on rolling grant no. PPA/G/O/2001/00482. RJMcL acknowledges the support of the Royal Society, through the award of a Royal Society URF.

## REFERENCES

- Arnouts S. et al., 2001, *A&A*, 379, 740
- Bertin E., Arnout S., 1996, *A&AS*, 117, 393
- Bouwens R. J., Illingworth G., 2006, *New Astron. Res.*, 50, 152
- Bouwens R. J. et al., 2004, *ApJ*, 616, L79
- Bouwens R. J., Illingworth G. D., Blakeslee J. P., Franx M., 2006, *ApJ*, 653, 53
- Bremer M. N., Lehnert M. D., Waddington I., Hardcastle M. J., Boyce P. J., Phillipps S., 2004, *MNRAS*, 347, L7
- Bruzual G. A., Charlot S., 2003, *MNRAS*, 344, 1000
- Bunker A. J., Stanway E. R., 2004, online-only reference (astro-ph/0407562)
- Bunker A. J., Stanway E. R., Ellis R. S., McMahon R. G., McCarthy P. J., 2003, *MNRAS*, 342, L47

- Calzetti D., Armus L., Bohlin R. C., Kinney A. L., Kooruneef J., Storchi-Bergmann T., 2000, *ApJ*, 533, 682
- Caputi K. I., Dunlop J. S., McLure R. J., Roche N. D., 2004, *MNRAS*, 353, 30
- Caputi K. I., Dunlop J. S., McLure R. J., Roche N. D., 2005, *MNRAS*, 361, 607
- Caputi K. I., McLure R. J., Dunlop J. S., Cirasuolo M., Schael A. M., 2006, *MNRAS*, 366, 609
- Chabrier G., 2003, *PASP*, 115, 763
- Cirasuolo M. et al., 2006, *MNRAS*, submitted (astro-ph/0609287)
- Cole S. et al., 2001, *MNRAS*, 326, 255
- Dickinson M. et al., 2004, *ApJ*, 600, L99
- Doherty M., Bunker A. J., Ellis R. S., McCarthy P. J., 2005, *MNRAS*, 361, 525
- Eyles L. P., Bunker A. J., Stanway E. R., Lacy M., Ellis R. S., Doherty M., 2005, *MNRAS*, 364, 443
- Grazian A. et al., 2006, *A&A*, 449, 951
- Heavens A. F., Panter B., Jimenez R., Dunlop J. S., 2004, *Nat*, 428, 625
- Jimenez R., MacDonald J., Dunlop J. S., Padoan P., Peacock J. A., 2004, *MNRAS*, 349, 240
- Madau P., 1995, *ApJ*, 441, 18
- McLure R. J. et al., 2006, *MNRAS*, 372, 357
- Mandelbaum R., Seljak U., Kauffman G., Hirata C. M., Brinkmann J., 2006, *MNRAS*, 368, 715
- Mobasher B. et al., 2005, *ApJ*, 635, 832
- Nagamine K., Cen R., Furlanetto S. R., Hernquist L., Night C., Ostriker J. P., Ouchi M., 2006, *NewAR*, 50, 29
- Oke J. B., Gunn J. E., 1983, *ApJ*, 266, 713
- Ouchi M. et al., 2005, *ApJ*, 620, L1
- Panagia N., Fall S. M., Mobasher B., Dickinson M., Ferguson H. C., Giavalisco M., Stern D., Wiklind T., 2005, *ApJ*, 633, L1
- Roche N. D., Dunlop J. S., Caputi K. I., McLure R. J., Willott C. J., Crampton D., 2006, *MNRAS*, 370, 74
- Shioya Y. et al., 2005, *PASJ*, 57, L33
- Somerville R. S., 2005, in Bender R., Renzini A., eds, *Multiwavelength Mapping of Galaxy Formation and Evolution*, Springer-Verlag, Berlin, p. 131
- Stanway E. R. et al., 2004, *ApJ*, 604, L13
- Stark D. P., Bunker A. J., Ellis R. S., Eyles L. P., Lacy M., 2006, *ApJ*, in press (astro-ph/0604250)
- Taniguchi Y. et al., 2005, *PASJ*, 57, 165
- Vanzella E. et al., 2005, *A&A*, 434, 53
- Vanzella E. et al., 2006, *A&A*, 454, 423
- Willott C. J., Rawlings S., Jarvis M. J., Blundell K. M., 2003, *MNRAS*, 339, 173
- Wolf C. et al., 2004, *A&A*, 421, 913
- Yan H. et al., 2005, *ApJ*, 634, 109

This paper has been typeset from a  $\text{\TeX}/\text{\LaTeX}$  file prepared by the author.